Streamer propagation in air in non-axially symmetric electric field

STREAMER PROPAGATION IN AIR IN NON-AXIALLY SYMMETRIC ELECTRIC FIELD

S. Singh[12*], Y. V. Serdyuk[1], R. Summer[2]
[1]Chalmers University of Technology, 41296 Gothenburg, Sweden
[2]Schneider Electric, Rathenaustrasse 2, 93051 Regensburg, Germany
*Email: singhs@chalmers.se

Abstract: Development of non-axial streamer discharges in air between disc-electrodes is studied. Discharge inception and propagation between edges of two flat discs is treated with so-called drift-diffusion model accounting for transport, generation and losses of electrons and two generic types of ions (positive and negative) under the influence of the electric field. To simulate propagation of a streamer channel, generation of secondary electrons at the streamer head due to photoionization is included. Partial differential equations constituting the model are solved utilizing custom developed stabilized finite element procedure implemented in commercial software. The results of the performed simulations show that discharge inception takes place in the regions of enhanced electrostatic fields at the curved edges of both electrodes and two streamers propagate in air gap towards each other. Quantitative analysis of the dynamics of charge carriers' densities, generated space charges and magnitudes of the electric fields during streamer initiation and propagation is presented. The effect of space charges and their influence on the streamer propagation path is discussed.

1 INTRODUCTION

Streamer type electrical discharges in high voltage gas insulated systems are critical from the design point of view for the apparatus to withstand operating and test voltage levels. Thus in medium voltage gas insulated switchgears (GIS), there are many locations with sharp edges and curved surfaces of conductors that, being exposed to high voltages, may provide conditions for inception of streamers. The discharge is triggered by free electrons in gas gaining enough energy in the electric field to initiate impact ionization of neutral species. The ionization process is exponential in nature and leads to development of electron avalanches on early stages of a discharge which can be further transformed to a streamer. For this, an avalanche needs to be sufficiently strong and produce high number of free charge carriers. At high pressures and locally enhanced fields typical for GIS, the charge generation rate in primary avalanches may become so high that significant space charge can be generated capable to modify the electric field and thus causing streamer initiation. Further, depending on the strength of the background field, streamer channel can propagate for a significant distance and bridge the gap between the electrodes leading to a partial or complete breakdown.

Streamer discharges have been a subject of numerous investigations including those based on advanced computer simulations. For the latter, development of streamers was typically considered in symmetrical electrodes arrangements, e.g., point-plane, needle-plane, coaxial cylinders, etc., which, however, are far from being representative for practical GIS designs. The simple systems always suggest a path for discharges and breakdowns along the shortest distance between electrodes coinciding with the geometrical symmetry axis that is seldom the case in real situations. In the paper, streamer development between the edges of two flat circular discs is analyzed following the approach reported in [1, 2].

2 THE MODEL AND ITS IMPLEMENTATION

Transport of charged species through neutral gas in an electric field **E** is considered using so-called drift-diffusion model [3] which consists of mass conservation equations for charge carriers coupled with Poisson's equations for electric potential *V* :

$$\partial N_{\mathrm{e}}/\partial t + \nabla \cdot (-N_{\mathrm{e}}\mathbf{w}_{\mathrm{e}} - D_e \nabla N_e) = R_e \qquad (1)$$

$$\partial N_p/\partial t + \nabla \cdot \left(N_p \mathbf{w}_{\mathrm{p}} - D_p \nabla N_p\right) = R_p \qquad (2)$$

$$\partial N_n/\partial t + \nabla \cdot (-N_n \mathbf{w}_{\mathrm{n}} - D_n \nabla N_n) = R_n \qquad (3)$$

$$(-\epsilon_0 \epsilon_{\mathrm{r}} \nabla V) = q\left(N_p - N_e - N_n\right) \qquad (4)$$

Here, subscripts *e*, *p* and *n* indicate electrons and generic positive and negative ions, respectively; *N* stands for the density, m^{-3}; *t* is time, s; $\mathbf{w} = \mu \mathbf{E}$ is the drift velocity vector, m/s, and μ is the mobility, m^2/Vs; *D* stands for the diffusion coefficient, m^2/s; ϵ_0 is the permittivity of vacuum, F/m; ϵ_{r} is the relative permittivity; *q* is the elementary charge, C. Note that the right hand side of (4) is essentially a density of the space charge, C/m^3, and solution of the equation yields the electric field $\mathbf{E} = -\nabla V$, V/m. The terms *R* on the right hand sides of equations (1)-(3) represent net rates of particles generation and loss processes. Thus, finite densities of

charged species at zero applied fields exist in air due to natural ionizing processes like terrestrial radiation, cosmic rays, etc., the intensity of which is characterised by the rate R_0 , $m^{-3}s^{-1}$. In strong applied fields, electron impact ionization of neutral molecules acts as a source of electrons and positive ions and its rate is introduced as a product $R_{ion} = \alpha N_e |w_e|$, where α is Townsend's ionization coefficient, m^{-1}, and $|w_e|$ stands for the magnitude of electrons drift velocity. Free electrons can be captured by electronegative components of air (O_2, CO_2, H_2O) and, therefore, the rate of electron attachment $R_{att} = \eta N_e |w_e|$ (here, η stands for the attachment coefficient, m^{-1}) is to be accounted for as a source term in equation (3) for negative ions and as a loss term in (1). The rate of the inverse process (detachment of electrons from negative ions) is introduced as $R_{det} = k_{det} N_e N_n$, where k_{det} is the corresponding coefficient, m^3/s. Charged species carrying charges of opposite signs can disappear in reactions of recombination the rates of which are proportional to the product of their densities and are defined by corresponding coefficients β , m^3/s. Thus, the rates of electron-ion and ion-ion recombination are $R_{ep} = \beta_{ep} N_e N_p$ and $R_{pn} = \beta_{pn} N_p N_n$, respectively. In addition, the rate of photoionization R_{ph} is to be considered. Accounting for the processes relevant to each kind of charges species, the terms on the right hand sides of (1)-(3) can be represented as

$$\begin{aligned} R_e &= R_{ion} + R_{det} + R_0 + R_{ph} - R_{att} - R_{ep} \\ R_p &= R_{ion} + R_0 + R_{ph} - R_{ep} - R_{pn} \\ R_n &= R_{att} - R_{det} - R_{pn} \end{aligned} \quad (5)$$

Photoionization is a process supporting streamer propagation in air by creating a localized source of electrons just in front of the streamer head. It is commonly accepted today [4] that the mechanism of photoionization in air is connected to photons generated by quenching of exited states of nitrogen molecules. Such exited species are capable to ionize oxygen molecules since the energy of irradiated photons is higher than the ionizations threshold of O_2. The local photoionization rate at a given point in discharge volume is a sum of all the volumetric photoionization events caused by photons travelling through the medium which is characterized by certain absorption coefficient. An integral method for calculating photoionization rate has been proposed in [4]. This approach, however, is extremely computationally expensive due to non-local character of the process (photons ionize molecules at locations different from that where they are generated). Recently, highly efficient differential method based on solution of Helmholtz equations was suggested [5] according to which the photoionization rate is given as a sum (6) of solutions of equations (7):

$$R_{ph} = \sum_i R_{ph}^i \quad (6)$$

$$\nabla^2 R_{ph}^i(\mathbf{r}) - \left(\lambda_i \mathrm{p_{O_2}}\right)^2 R_{ph}^i(\mathbf{r}) = -\mathrm{A}_i \mathrm{p_{O_2}}^2 \mathrm{I}(\mathbf{r}) \quad (7)$$

Here, $\mathrm{p_{O_2}}$ is partial pressure of oxygen and $\mathrm{I}(\mathbf{r})$ is the photons generation rate. Index i represents the number of components contributing to the total photoionization rate. In the present study, three-term approximation is chosen following [6]. The rate $\mathrm{I}(\mathbf{r})$ is given by equation (8), where $\mathrm{p_q}$ represents the quenching pressure (which is equal to 60 Torr) and ξ is the efficiency of the process:

$$\mathrm{I}(\mathbf{r}) = \mathrm{p_q} \xi R_{ion} / (\mathrm{p_{O_2}} + \mathrm{p_q}) \quad (8)$$

Model parameters used in the present study are adopted from [1-3] and are listed in Table1. Dependences of the reduced ionization α/N and attachment η/N coefficients on reduced electric field strength E/N, Td, are shown in Figure 1 (N stands for gas density, m^{-3}, for given pressure and temperature). The drift velocity and diffusion coefficient of electrons are approximated as

$$\mathrm{w_e} = 3.2 \cdot 10^3 (E/N)^{0.8} \quad (9)$$

$$\mathrm{D_e} = 7 \cdot 10^{-2} + 8\,(E/N)^{0.8} \quad (10)$$

The model equations were complemented with boundary and initial conditions following [1-3] and

Table 1: Parameters used in the simulation

Parameters	Values
μ_p , m^2/Vs	$2 \cdot 10^{-4}$
D_p , $m^2\,s^{-1}$	$5.05 \cdot 10^{-6}$
μ_n , m^2/Vs	$2.2 \cdot 10^{-4}$
D_n , $m^2\,s^{-1}$	$5.56 \cdot 10^{-6}$
β_{ep}, $m^3\,s^{-1}$	$5 \cdot 10^{-14}$
β_{pn} , $m^3\,s^{-1}$	$2.07 \cdot 10^{-12}$
R_0 , $m^{-3}\,s^{-1}$	$1.7 \cdot 10^{9}$
k_{det} , $m^3\,s^{-1}$	10^{-18}

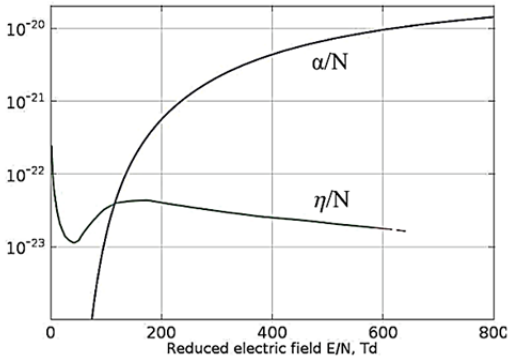

Figure 1: Ionization and attachment coefficients as functions of the reduced electric field.

were implemented in Comsol Multiphysics software. To insure positivity of the solution of the drift-diffusion equations (1)-(3), they were converted into a logarithmic form and were implemented using customized weak formulation stabilized by introducing a test function similar to streamline diffusion with shock capturing. Adaptive mesh refinement was applied by splitting the base mesh in regions with sharp gradients of species concentrations and fields on each time step. This allowed for resolving properly streamers heads as well as for reducing computational time. The electrode boundaries were resolved with finer static mesh to accurately capture flux transfer. An implicit time stepping technique based on backward differential formula was used. The dependent variables were segregated in two groups and iteratively converged for each time step by utilizing continuous Jacobian update.

3 NON-AXIAL STREAMERS PROPAGATION

The model was tested and verified by conducting simulations of a nanosecond discharge in needle-plane geometry and by comparing calculated and experimental results [1]. In addition, simulations of development of streamers of different length were performed following [2]. In both cases, the presented model provided results which were in agreement with the reference data and demonstrated high performance in terms of computational time and stability.

After testing and verification, simulations of non-axially symmetric streamer discharge in air at atmospheric pressure and room temperature were conducted. The discharge was considered to be initiated between disc-shaped electrodes 10 mm in diameter with rounded edges (radius 0.5 mm) separated by a distance of 10 mm. Positive DC step potential of 35 kV was applied to the top electrode while the other one was grounded. The problem was reduced to two dimensions utilizing axial symmetry of the electrode system. In reality, the problem is three-dimensional since the discharge is initiated at a location with strongest field and propagates in a filamentary form. In the simulations, an ideal situation is considered assuming that probabilities of discharge inception are equal for each point on the edges of the electrodes. Boundary conditions for the drift-diffusion equations (1)-(3) were implemented specifying outward particles fluxes when the charged species were moving towards electrode's surface whereas zero flux boundary conditions were used when charge carriers were drifting into the gas volume away from the boundary. On all other boundaries, zero fluxes were implemented. The boundary conditions for (7) were of Dirichlet type with zero values on all boundaries [5]. Adaptive mesh refinement was implemented based on L2-norm of the gradient of electron density.

The calculated electron density patterns at streamer initiation and propagation are shown in Figure 2. As seen, streamer inception takes place in the region with the strongest electric field at the curved surface of the positive energized electrode. During first few nanoseconds, the discharge channel expands and then starts moving towards the grounded electrode. The peak of electrons density during propagation reaches ~10^{15} cm^{-3}, as

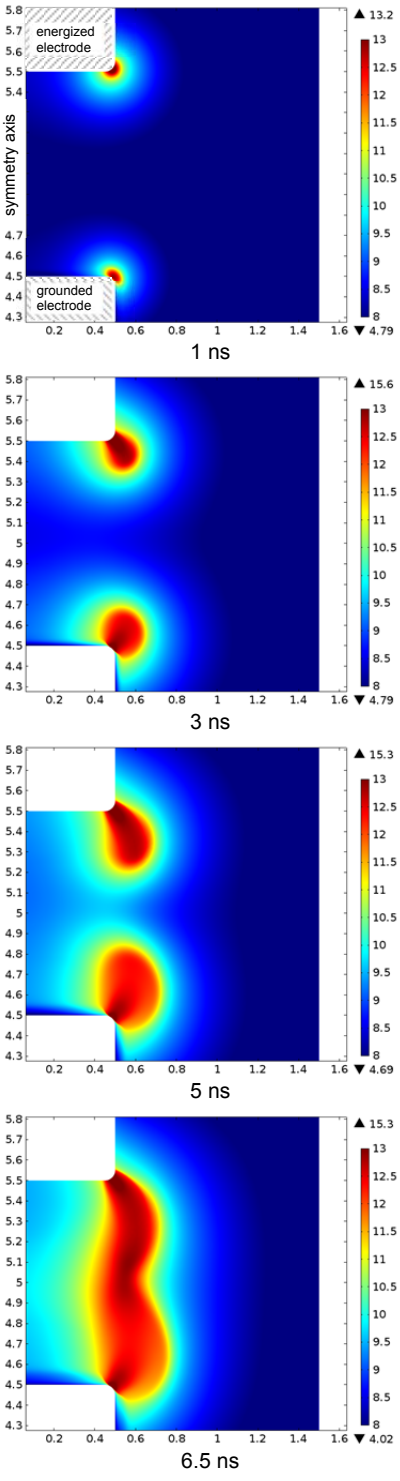

Figure 2: Distributions of electron density (cm^{-3}, log scale) at different time after voltage application.

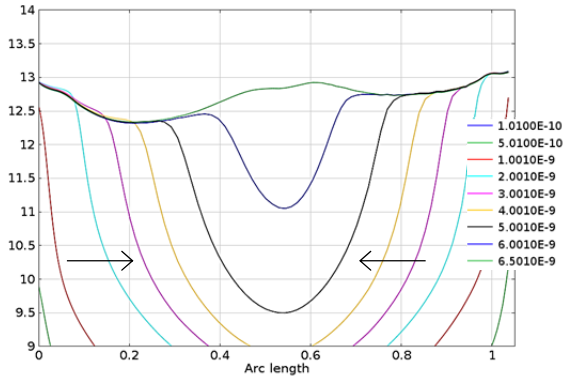

Figure 3: Log of electron density (cm^{-3}) along streamer axis over time (shown in the legend, s). Arrows indicate directions of propagation. The abscissa is accounted from the edge of the positive electrode.

seen in Figure 3, that is similar in magnitude to axial streamers [2]. As observed in Figure 2, after ~5 nanoseconds, positive streamer channel starts deviating from its initial trajectory turning inward, towards the axis. The negative streamer inception also starts at the same instant of time, due to homogenous field distribution about the horizontal mid plane of the domain. Initially the negative streamer follows the initial background field line but deviates from it at ~5 nanoseconds. Further, the streamers move towards each other and finally meet forming a continuous channel bridging the gap between the electrodes. At this stage, the peak electron density reaches ~10^{15} cm^{-3}. From the profiles in Figure 3, the averaged velocities of the propagating fronts are ~$1.5 \cdot 10^{8}$ cm/s for both positive and negative streamers.

The electric field distributions for different time moments are plotted in Figure 4. One can notice that streamers heads are properly resolved and the peak electric field magnitude reaches ~ 80 kV/cm. The field strength is highest in the narrow regions at the streamers heads and lowest behind them. This is reflected in the distributions in Figure 5 where characteristic peaks of the field associated with the fronts of the discharges moving from the electrodes are observed. These can be considered as ionization waves converting neutral gas to discharge plasma with a relatively high electron density as indicated in Figures 2 and 3. The resulting conductivity of the channels is high (~100 mS/m) as compared to the neutral gas that causes the drop of the field strength behind the advancing discharge fronts. During propagation, the peak field remains fairly stable in magnitude (see curves for the range 1 – 6.5 ns in Figure 5) until the positive and negative streamers approach each other. After that moment, a single local peak appears and the field pattern becomes quite complex as seen in Figure 4 for the instant 6.5 ns. In general, the level of the field strength (associated with the head and within the channel)

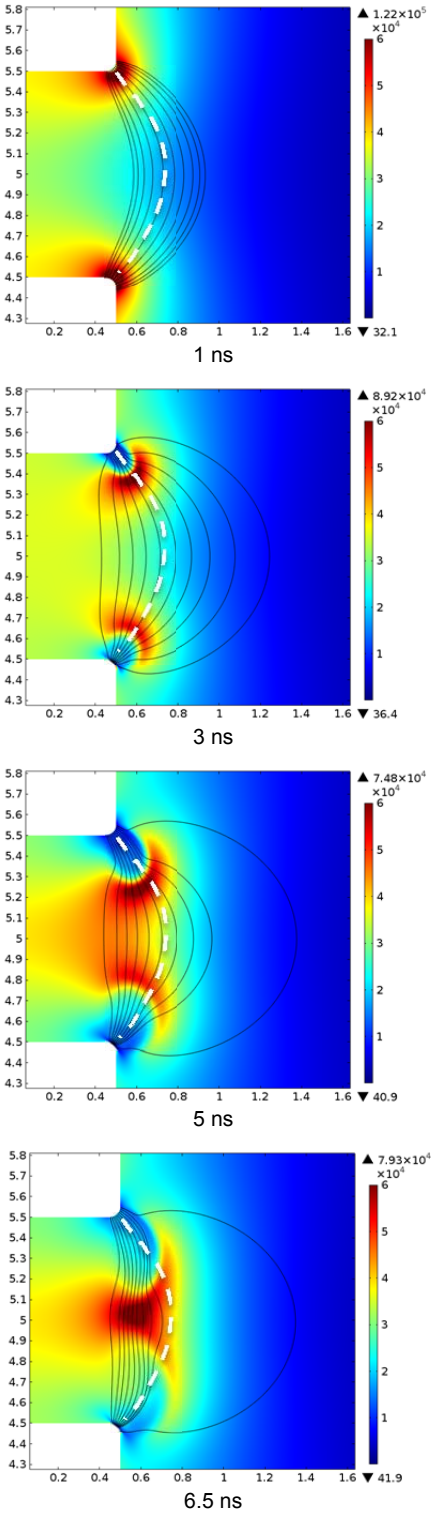

Figure 4: Electric field (V/cm) patterns at different instants after voltage application. The black lines indicate electric field lines. The dashed line indicates initial background electrostatic field line.

and the electron densities computed for the individual streamers agree well with the characteristics obtained from simulations of axially propagating streamers, see e.g. [7, 8]. An interesting observation in Figures 2 and 4 is that positive streamer, being initiated at the point of the strongest field on the edge of the energized

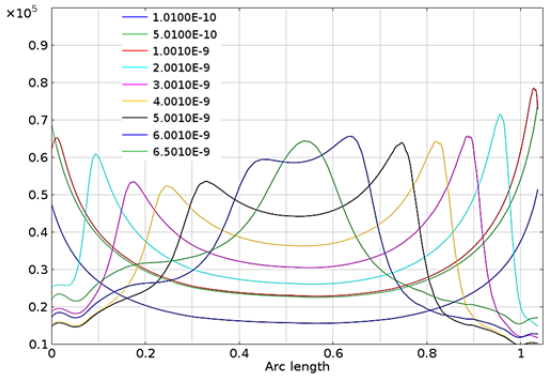

Figure 5: Electric field magnitude (V/cm) along streamer axis over time (shown in in seconds).

positive electrode, propagates along a line of the electrostatic field (indicated by the dashed line in Figure 4) originating from the same point, see plots for 1 ns. The inception of the negative streamer takes place at the location of the strongest field on the counter electrode as seen in the plot for 1 ns. On later stages, however, electrostatic interaction of the space charges created behind both propagating fronts causes deviations of the trajectories of the streamers from the electrostatic field line as observed in the plots for 5 ns and 6.5 ns. By merging of the channels, a path is created along which a spark leading to a complete breakdown may occur depending upon properties of the external circuit. The deviation of this path from the electrostatic field line may results in significant errors when trying to apply well-known empirical streamer breakdown criteria for evaluations of breakdown voltages. Note that this problem inherently occurs in most practical cases, where streamer propagation does not take place along the shortest geometric distance between electrodes. The latter is typical for axisymmetric arrangements like point-plane or needle-plane only, which are rather rear in practice. In cases when solid insulating elements are incorporated into gas, uncertainties in choosing the breakdown path are even more significant [9, 10] and can be cleared by conducting simulations of discharges based on the approach presented above.

4 CONCLUSION

Customized drift-diffusion model of a streamer discharge in atmospheric pressure air have been implemented in commercial software and simulations of non-axial streamer discharges between disks electrodes have been conducted. The results demonstrated that the discharge process involved development of two streamers originating from edges of both electrodes and propagating towards each other. The properties of the streamers were found to be similar to that of axial discharges reported in literature. It was observed that interaction between space charges associated with the streamers heads led to deviations of their trajectories from the electrostatic field line. Such deflections should be taken into account when applying empirical streamer breakdown criteria for evaluations of breakdown voltages in most practical cases when pre-breakdown discharges do not occur along the shortest geometrical distance between electrodes.

REFERENCES

[1] S. Singh, Y. V. Serdyuk and R. Summer, "Adaptive Numerical Simulation of Streamer Propagation in Atmospheric Air" COMSOL Conf., Rotterdam, Netherlands, 2013.

[2] Y. V. Serdyuk, "Propagation of Cathode-Directed Streamer Discharges in Air" COMSOL Conf., Rotterdam, Netherlands, 2013.

[3] Y. V. Serdyuk, "Numerical Simulations of Non-Thermal Electrical Discharges in Air", in Lightning Electromagnetics, ed. V. Cooray, IET, London, UK, pp. 87-138, 2012.

[4] M. B. Zhelezniak, A. K. Mnatsakanian, and S. V. Sizykh, "Photoionization of Nitrogen and Oxygen Mixtures by Radiation from Gas Discharge," High Temperature, Vol. 20, pp. 357–362, 1982.

[5] A. Bourdon, V. P. Pasko, N. Y. Liu, S. Célestin, P. Ségur, and E. Marode, "Efficient Models for Photoionization Produced by Non-Thermal Gas Discharges in Air Based on Radiative Transfer and the Helmholtz equations," Plasma Sources Sci. Technol., Vol. 16, pp. 656-678, 2007.

[6] G. Wormeester, S. Pancheshnyi, A. Luque, S. Nijdam, and U. Ebert, "Probing Photo-Ionization: Simulations of Positive Streamers in Varying N2 : O2 Mixtures," J. Phys. D: Appl. Phys., Vol. 43, p. 505201, 2010.

[7] G. E. Georghiou, A. P. Papadakis, R. Morrow, and A. C. Metaxas, "Numerical Modelling of Atmospheric Pressure Gas Discharges Leading to Plasma Production," J. Phys. D: Appl. Phys., Vol. 38, pp. R303-R328, 2005.

[8] R. Morrow and J. J. Lowke, "Streamer Propagation in Air," J. Phys. D: Appl. Phys., Vol. 30, 1997.

[9] A. Pedersen, T. Christen, A. Blaszczyk, and H. Boehme, “Streamer Inception and Propagation Models for Designing Air Insulated Power Devices”, Ann Rep. 2009 IEEE Conf. Elec. Insul. Diel. Phenomena, Oct. 19-21, 2009, Virginia Beach, USA, pp.604-607.

[10] M. Ramesh, R. Summer, S. Singh, Y. V. Serdyuk, S. M. Gubanski, and S. Kumara, “Application of Streamer Criteria for Calculations of Flashover Voltages of Gaseous Insulation with Solid Dielectric Barrier”, Proc. 18th Int. Symp. High Voltage Eng., Aug. 25-30, 2013, Seoul, Korea, pp.1258-1263.